Pergamon

Journal of Structural Geology, Vol. 19, No. 11, pp. 1359 to 1368, 1997

PII: S0191-8141(97)00050-3
0191-8141/97 $17.00 + 0.00

Fluid inclusions in crack–seal veins at Dugald River, Mount Isa Inlier: implications for palaeostress states and deformation conditions during orogenesis

GUOJIAN XU

Department of Earth Sciences, James Cook University, Townsville, Qld 4811, Australia

(*Received* 28 *February* 1996; *accepted in revised form* 5 *June* 1997)

Abstract—An integrated geometrical investigation and microthermometric analysis of fluid inclusion trails in fibrous crack–seal veins at Dugald River, Mount Isa Inlier, allowed distinction of two general types of fluid inclusions: a $CO_2 \pm CH_4$-rich variety and a H_2O-rich variety. At least three stages of fluid percolation are identified to be related to the vein formation. Trails of pseudosecondary inclusions have a constant orientation relative to the direction of the regional maximum principal shortening direction (λ_3). This relationship allows the trails to be regarded as potential structural markers. However, trails of secondary inclusions generally show a deviation from the established bulk shortening direction and possibly reflect the overprinting of a later deformation event. Microthermometric data combined with knowledge of metamorphic reactions suggest that the P–T path of crack–seal deformation started at about 450°C and 2.8 kbar, then crossed 340°C and 1.2 kbar, and possibly terminated around 130°C and at near-surface pressure, corresponding to the regional crustal uplift. This study shows the importance of combined geometrical and microthermometric studies of fluid inclusions for understanding the physical conditions of crack–seal deformation, a common phenomenon in low-grade metamorphic terrains.

INTRODUCTION

During the last 10 years, much work has been done on relations between fluid inclusion trails and regional stress fields (Pecher *et al.*, 1985; Lespinasse and Pecher, 1986; Kowallis *et al.*, 1987; Laubach, 1989; Ren *et al.*, 1989; Alvarenga, 1990; Cathelineau *et al.*, 1990; Boullier *et al.*, 1991; Boiron *et al.*, 1992; Boullier and Robert, 1992; Selverstone *et al.*, 1995). The coherent behaviour of fluid inclusion orientations relative to the macroscopic structure provides independent strain markers to unravel a rock's deformation history. By looking at fluid inclusions within healed microcracks, Pecher *et al.* (1985) and Lespinasse and Pecher (1986) were able to demonstrate that the inclusion trails were directly related to distinct deformation events. Kowallis *et al.* (1987), Laubach (1989), Ren *et al.* (1989), Cathelineau *et al.* (1990) and Boullier *et al.* (1991) have emphasized the use of fluid inclusion trails for relating the different stages of fluid percolation in crystalline rocks to a regional succession of deformation episodes and establishing the palaeostress fields involved. Fluid inclusion trails have also been used as a reliable indicator of ore fluid pathway by correlating the geometry of microstructural markers with the time–space relationships between deformation events, mineral healing, fluid trapping and ore deposition (Boiron *et al.*, 1992). In addition, geothermal chronology established on oriented fluid inclusion planes has been successfully applied to constrain fault kinematics (Selverstone *et al.*, 1995).

However, previous fluid inclusion studies in this field were almost exclusively conducted on secondary inclusions; that is, those that form by healing microfractures developed after the growth of the host crystal (Roedder, 1984). Fluids trapped in these secondary inclusions do not reflect the physicochemical conditions under which the host mineral crystallizes. In contrast, samples collected from crack–seal fibrous veins in the Dugald River area of the Mount Isa Inlier provide an uncommon opportunity to examine pseudosecondary inclusions. Crack–seal fibrous veins also provide an ideal case for studying the role of fluids in their formation, related physical conditions and their changes with time (Roedder, 1984; Mullis, 1987). The present study was undertaken to investigate the preferred orientations of fluid inclusion trails vs regional palaeostress states, and to obtain fluid inclusion data which can be used to constrain the temperature–pressure path of vein formation during orogenesis.

GEOLOGICAL SETTING

The study area is located in the northeastern portion of the Middle Proterozoic Mount Isa Inlier, northwest Queensland (Fig. 1). It contains the Dugald River Zn–Pb–Ag deposit, which is hosted by graphitic black slates. The regional sedimentary sequence comprises a thick package of variably calcareous, argillitic and siliciclastic sediments of the Corella Formation (Blake, 1982), Lady Clayre Dolomite and Knapdale Quartzite (Derrick *et al.*, 1977). These have been interpreted as sag phase sediments deposited within the Cloncurry Basin (Beardsmore *et al.*, 1988). The whole succession was subjected to upper greenschist to middle amphibolite facies metamorphism (Newbery *et al.*, 1993) during the second deformation.

Recent structural work (Xu, 1996) has shown that there are six deformation episodes in the Dugald River area. D_1 produced approximately E–W-trending folds and a locally pervasive foliation, with associated late-

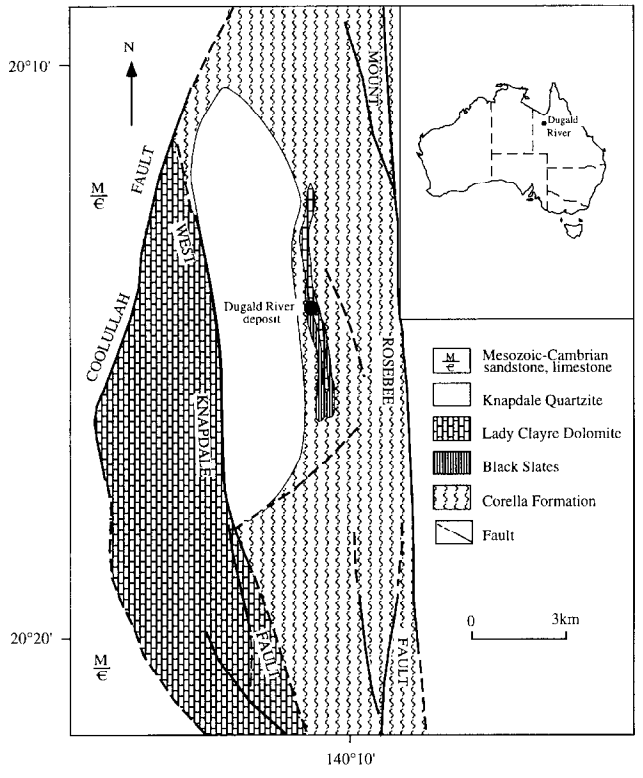

Fig. 1. Simplified geological map and location of the Dugald River area.

stage, N–S-striking faults. D_2 was the dominant deformation event and produced regional tight to isoclinal folds with steep N–S-striking axial planes and a well-developed S_2, resulting from E–W compression (Holcombe *et al.*, 1991, 1992; Oliver *et al.*, 1991; Reinhardt, 1992). D_3 generated local small-scale folds with subhorizontal axial planes and associated weak cleavage. D_4 is characterized by outcrop-scale folds and crenulations with near N–S-oriented axial planes, plus narrow shear zones. D_5 occurs as sporadic kinks, and D_6 formed E–W-trending open folds and associated conjugate strike-slip faults. The first four deformation events were generated in a ductile regime, whereas the last two were transitional (D_5) to brittle deformation (D_6). Relationships of mineralization with folds and cleavage indicate a post-D_2 timing for the Zn–Pb–Ag deposit at Dugald River (Xu, 1996). In general, the development of crack–seal veins is closely related to the D_2 deformation over the study area, although some exceptions can be found associated with other deformation events.

Within the Dugald River area, crack–seal fibrous veins are abundant in the Lady Clayre Dolomite but extremely rare in outcrops of the biotite scapolite schist of the Corella Formation and the Knapdale Quartzite. This lithological preference is possibly due to the difference in rock competence (Ramsay and Huber, 1983). The Lady Clayre Dolomite forms prominent outcrops of black, argillaceous and limey metasediments. The major lithotypes are dolomite and dolomitic siltstone interbedded with thin black cherty layers (Newbery *et al.*, 1993). The mineralogy is dominated by calcite, dolomite and quartz with subordinate mica, graphite and chlorite. Scapolite and K-feldspar porphyroblasts are common and aligned parallel to the S_2 cleavage.

VEIN GEOMETRY AND MORPHOLOGY

The veins examined in this study generally lie at a high angle to the dominant N–S-trending S_2 foliation and maintain a constant subvertical orientation throughout the study area (Fig. 2). Their overall orientation is consistent with a regional E–W compression direction during D_2. In some cases, veins of this type show strong dissolution of vein minerals along vein walls due to strain accumulation on vein margins, which was caused either by the progressive deformation of the D_2 event or the subsequent D_4 deformation. Based on the overprinting relations between veins and deformation fabrics of D_2 and D_4, a syn-post D_2 formation is proposed. The same timing of such veins has been determined elsewhere in the Mount Isa Inlier (Winsor, 1983; Valenta, 1989; Oliver *et al.*, 1991; Reinhardt, 1992; Valenta *et al.*, 1994).

The vein-filling minerals are almost invariably dominated by calcite, dolomite and fibrous quartz. Most of the veins are 100–300 cm long and 3–5 cm thick, with individual veins as thick as 10 cm. Fibres are usually oriented perpendicular to the vein walls, although oblique fibres can occur. Most of the veins typically demonstrate syntaxial growth (i.e. the material filling the vein is compositionally similar to that of vein walls; Ramsay and Huber, 1983) with fibrous, crack–seal morphologies similar to those described by Ramsay (1980).

ORIENTATION OF FLUID INCLUSION TRAILS

The trails of fluid inclusions investigated in this study consist of healed intracrystal and transcrystal microcracks (Fig. 3). Combined with the consideration of the inclusion morphology, healed intracrystal microcracks

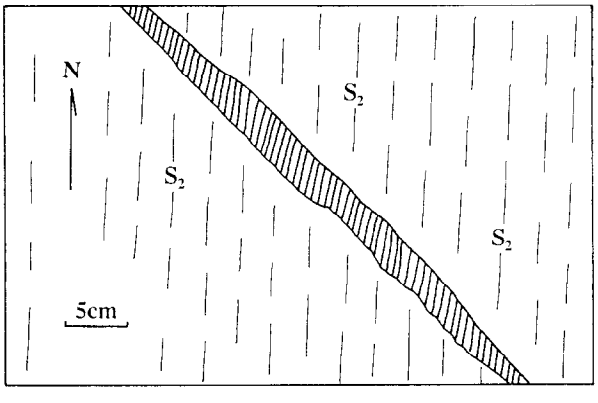

Fig. 2. Sketch from a photograph (plan view) showing a crack–seal vein lying at a high angle to S_2 foliation in the Lady Clayre Dolomite. Fibres are usually oriented perpendicular to the vein walls.

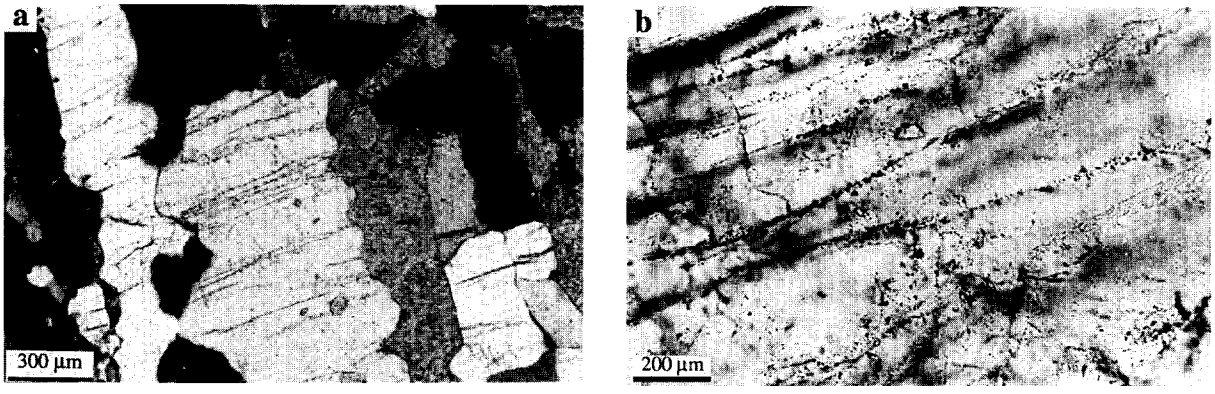

Fig. 3. (a) Photomicrograph showing near E–W-trending fluid inclusion trails formed by healing of the intracrystal and transcrystal fractures with respect to the boundaries of quartz fibre. Crossed nicols. Section is horizontally oriented. North is towards the top. (b) Close-up of pseudosecondary fluid inclusion trails, similar to those depicted in (a).

generally correspond to pseudosecondary inclusions, whereas healed transcrystal microcracks correspond to secondary inclusions (Roedder, 1984). Healed fractures are common in most of the examined samples but were only clearly observed in the fibrous quartz crystals. As I was mainly concerned with the correlation between fluid circulation and regional stress field during the propagation of crack–seal veins, only pure extensional cracks, without discernible lateral displacement, were counted in the statistics presented here, even though exceptions resulting from shear failure cannot be effectively ruled out.

As most of the trails are nearly normal to the horizontal plane, orientations of fluid inclusion trails have been determined on horizontally oriented doubly polished sections from nine samples. Geometrically, almost all examined inclusion trails are either perpendicular or lie at a high angle to the long axes of the fibrous quartz crystals (Fig. 3). Systematic measurements of healed microcracks have been performed in each section by manual counting using a microscope. Results are expressed in the rose diagram (Fig. 4a) in which two main preferred orientations of fluid inclusion trails can be seen: a constant well-defined maximum around N75°E of set 1; and a less well-defined one around N115°E of set 2. The relative chronology of fluid inclusions, as inferred from petrographic observations, suggests that set 1 pre-dated set 2 and consists mainly of pseudosecondary inclusions, while set 2 is almost exclusively dominated by secondary inclusions cutting across crystal boundaries.

Trails of secondary fluid inclusions have been widely used as structural markers by previous workers, as approximating the average direction of maximum principal stress in the bulk rock (Pecher *et al.*, 1985; Lespinasse and Pecher, 1986; Kowallis *et al.*, 1987; Ren *et al.*, 1989; Boullier *et al.*, 1991). To test the reliability of the above interpretation in the alternative case of crack–seal fibrous veins, a regional strain state was established for the D_2 deformation event at Dugald River. As D_2 folds were formed by E–W bulk shortening (Holcombe *et al.*, 1991, 1992; Oliver *et al.*, 1991; Reinhardt, 1992), poles to axial plane cleavage should be parallel to the maximum principal shortening strain (Fig. 4b). Figure 4 clearly demonstrates a strong consistency between the regional bulk shortening and the orientations of set 1 fluid inclusion trails. This implies that local stress conditions were retained during the syntaxial overgrowth of fibrous crystals. Trails of these pseudosecondary inclusions are good indicators of the microstructural pattern at the time of crack–seal deformation, and are potentially as important as those in the bulk rock with regard to the deduction of the palaeostress state. Compared with set 1 trails, set 2 shows a clockwise rotation from the D_2 maximum principal stress direction. The absence of rotation of the D_2 fold axis suggests that a passive rotation of the sample relative to the regional coordinates is highly improbable. Given the constant relative cross-cutting relationship between set 1 and set 2 trails, the possibility that they are conjugate to each other can be discounted. Therefore, such deviation may represent the overprinting effect of subsequent deformation.

FLUID INCLUSION RESULTS

Analytical methods

Doubly polished sections, about 200 μm thick, were prepared from oriented vein samples. In general, no ductile deformation effects can be observed for the quartz fibres sampled for this study except the local presence of undulose extinction. The undeformed nature of the fibres suggests that fluid inclusions preserved in the crack–seal veins were trapped at or after peak deformation conditions. Fluid inclusion measurements were conducted on a Fluid Inc. adapted USGS gas flow heating and freezing stage. Generally, measurements were taken during heating of the sample at the rate of 5°C min^{-1}, but a heating rate of 1°C min^{-1} was employed in the vicinity of the phase change. The heating and freezing stage was calibrated at three temperatures: the critical point of water (374.1°C), the freezing point of water (0°C) and the

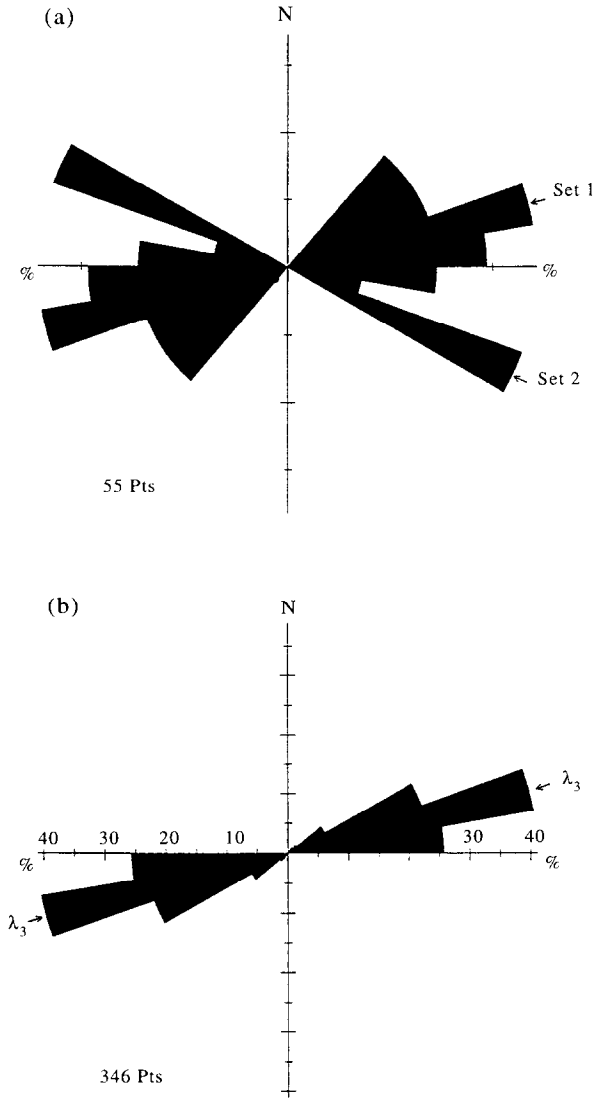

Fig. 4. (a) Rose diagram showing orientations of fluid inclusion trails for both pseudosecondary (set 1) and secondary (set 2) inclusions. (b) Rose diagram showing the maximum principal shortening direction (λ_3) of D_2. λ_3 was deduced from the orientation of the S_2 axial plane cleavage because D_2 folds are considered to be a result of E–W bulk shortening. By comparing (a) with (b), there is a strong consistency between the orientation of set 1 trails and the regional D_2 shortening direction.

triple point of carbon dioxide (−56.6°C) using synthetic standards. Measured temperatures have a reproducibility of ±0.1°C below 30°C, and ±1.0°C at temperatures around 375°C with a precision of ±0.2°C at all temperatures.

Fluid inclusion microthermometry

Petrographical examination revealed that fluid inclusions in the fibrous quartz crystals have widely varying compositions and several generations of fluid trapping. Based on the microthermometric results, two general types of fluid inclusions can be distinguished: one is $CO_2 \pm CH_4$-rich and the other is H_2O-rich. In most cases, both of them geometrically belong to the two pronounced orientations in the horizontal plane, referred to as set 1 and set 2, respectively, in the previous section.

$CO_2 \pm CH_4$-rich fluid inclusions. Fluid inclusions of this type are the major components of set 1 trails. In most cases, they were preferably aligned along healed microcracks (Fig. 5a), although isolated individuals can be locally observed (Fig. 5b). Fluid inclusions within this group are usually between 8 and 20 μm in size and show

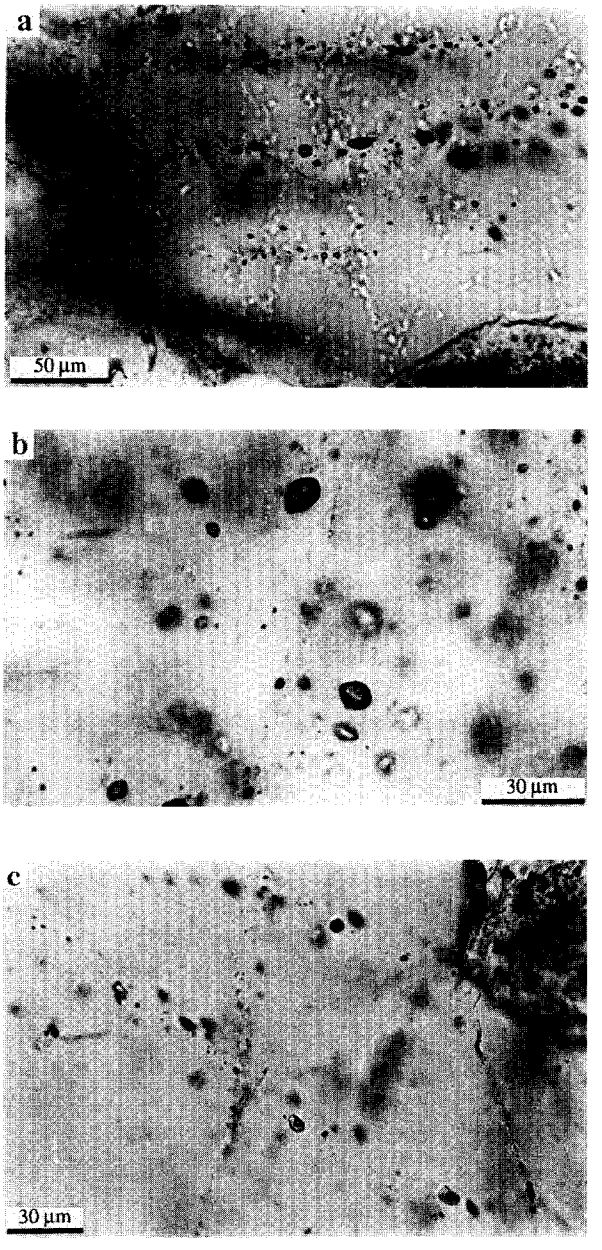

Fig. 5. (a) Photomicrograph of preferentially aligned two-phase (liquid CO_2 and vapour CO_2) and adjacent monophase carbonic inclusions which formed by the healing of intracrystal microcracks. Horizontally oriented section. North towards the top. (b) Photomicrograph of isolated carbonic inclusions with a typical negative crystal shape. They are monophase at room temperature, and probably primary in origin. (c) Photomicrograph of aqueous secondary inclusions present as decoration on the healed microcracks. At room temperature, they are two-phase liquid-rich. Section is horizontally oriented. North is towards the top.

oval to negative crystal shapes. At room temperature, many such fluid inclusions are monophase: hence, homogenization to the liquid phase is below room temperature. Liquid-rich two-phase inclusions were only found in set 1 trails. Melting temperatures of the solid CO_2 range from -60.8 to -56.4°C and show an asymmetric distribution toward temperatures below the triple point of pure CO_2 (Fig. 6a), indicating that variable amounts of CH_4 are present along with CO_2 in the inclusion, as was further confirmed by laser Raman spectroscopy. The presence of pure CO_2 inclusions was primarily recognized within the liquid-rich two-phase subgroup, with CO_2 melting temperatures near -56.6°C. Upon heating, all inclusions homogenize to liquid. Homogenization temperatures range from -12.9 to 29.1°C with a peak at 5°C (Fig. 6b). Using the graphical method presented by Shepherd *et al.* (1985), the maximum amount of CH_4 in these carbonic inclusions was estimated to be approximately 17 mol%. Signs of clathrate formation during cooling of the carbonic inclusions, which would suggest the presence of an aqueous fluid adhered to the inclusion walls, were not observed.

H_2O-rich fluid inclusions. Aqueous fluid inclusions, unlike carbonic inclusions, were found with variable abundance in almost all samples. Indeed, nearly all of the inclusions comprising set 2 trails and part of set 1 trails are of this type. Most such aqueous inclusions are present as decoration on the healed microcracks (Fig. 5c), but some samples do contain equant randomly dispersed inclusions. At room temperature, H_2O-rich inclusions consist of two phases: H_2O liquid and H_2O vapour with variable phase ratios throughout the examined sections but constant in a single trail. The size of H_2O-rich inclusions ranges from 5 to 25 μm.

Three subdivisions of the aqueous fluid inclusions can be made in terms of homogenization and melting temperatures (T_h and T_m), as well as occurrence. Also, petrographic observations indicate a clear relationship between the inclusion types and microfracture orientations, with subtype II confined to set 1 trails and subtype III in set 2 trails whereas subtype I appears to be overprinted by both trails (Fig. 7). Fluid inclusions of the first group usually occur as small isolated individuals and are primary in origin. At room temperature two phases are present in the inclusions, but relatively high vapour to liquid ratios exist throughout the investigated specimen. In spite of the uncertainty of their chronology relative to other aqueous inclusions, a large proportion of such inclusions can be more reasonably interpreted as earlier with respect to the peak deformation/metamorphism compared to both pseudosecondary and secondary aqueous inclusions discussed below. Most of these inclusions homogenize to liquid above 300°C with a peak at 315°C (Fig. 6c), while melting varies from -13 to -19°C (Fig. 6d).

Contrary to the above non-planar distribution of the

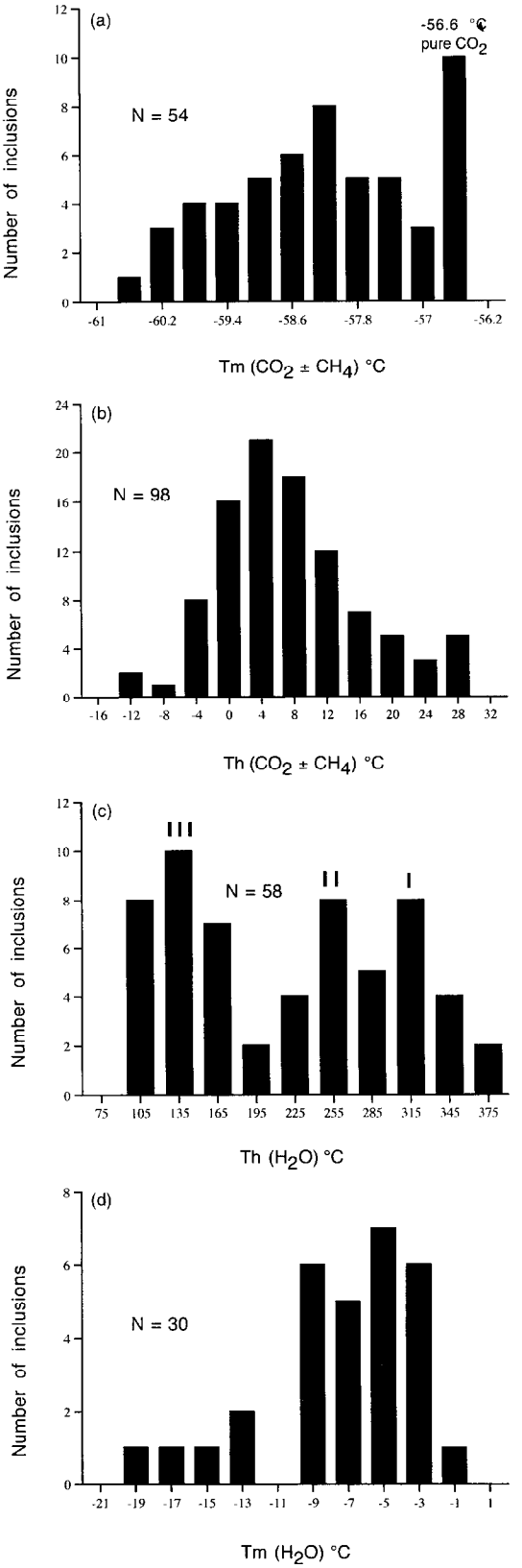

Fig. 6. Microthermometric data for fluid inclusions in quartz fibres. T_m ($CO_2 \pm CH_4$) = final melting temperature of CO_2 solid; T_h ($CO_2 \pm CH_4$) = homogenization temperature of CO_2 vapour to CO_2 liquid; T_m (H_2O) = final melting temperature of ice; T_h (H_2O) = homogenization temperature of H_2O vapour to H_2O liquid. Note that the three peaks demonstrated by the homogenization temperatures of aqueous inclusions sequentially correspond to the three different occurrences of inclusions illustrated in Fig. 7.

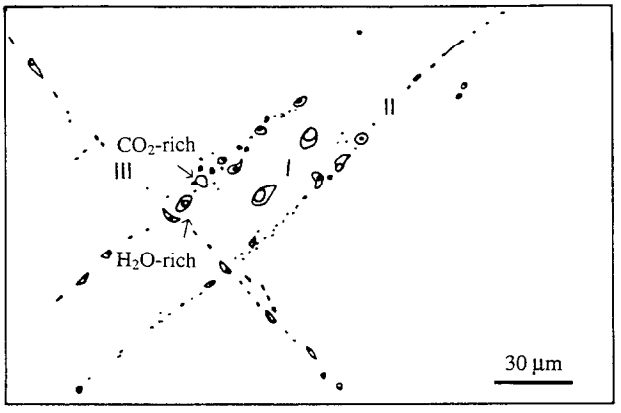

Fig. 7. Sketch from a photograph showing sequential fluid trapping during the growth of fibrous quartz. I, isolated primary inclusions formed in the early stage; II, pseudosecondary inclusions formed in the middle stage. Note the coexistence of monophase CO_2-rich inclusions and aqueous inclusions in the same intragranular trail, suggesting fluid immiscibility; III, secondary inclusions formed in the last stage. Horizontally oriented section. North towards the top.

first group of inclusions, the second and third groups of aqueous inclusions are present along distinct planes and lie in the set 1 and set 2 trails, respectively. In general, the second group inclusions have a pseudosecondary origin, characteristic of a peak homogenization temperature centred on 255°C (see Fig. 6c) and a final melting temperature peak at −9°C (see Fig. 6d). By contrast, aqueous inclusions of the third group generally homogenized at lower temperatures (102–185°C) and have a peak at 135°C (see Fig. 6c). Likewise, relatively high melting temperatures occur in the narrow range from −5 to −2°C (see Fig. 6d). In most cases, inclusions of this type cross-cut crystal boundaries and other intragranular trails and have an unequivocally secondary origin. They are, hence, thought to have formed after the later stage of syntectonic veining.

The initial melting temperatures of about −22°C for all aqueous inclusions indicate that NaCl is probably the dominant dissolved salt in the inclusion fluids. As a consequence, salinities are 17–21 wt% NaCl for the isolated aqueous inclusions, 9–13 wt% NaCl for inclusions with set 1 orientation and 3–7 wt% NaCl for those possessing set 2 orientation, based on freezing point depression (Bodnar, 1993).

In summary, fluid inclusions encountered in the crack–seal veins indicate that two compositionally (carbonic and aqueous) distinct fluids were trapped during the growth of fibrous quartz. This independent trapping of the two major components of an unmixed fluid apparently results from physical separation of the immiscible phases prior to trapping. Although several generations of H_2O-rich inclusions may be present in the same host mineral, textural evidence indicates that at least some aqueous inclusions (e.g. subtype II) were trapped simultaneously with the carbonic inclusions in the set 1 trails (see Fig. 7 for more details). Fluid inclusions for each type are both isolated and intracrystal, and even transcrystal with respect to fibre growth, suggesting they are syntectonic with respect to grain-boundary migration. Nevertheless, these growing fibres may trap fluid inclusions and preserve information on fluid compositions and densities during successive crack-forming events (Crawford and Hollister, 1986). Assuming that all inclusions preserved in the veins were trapped at or after peak deformation/metamorphism as stated in the previous section, the high-density carbonic inclusions and the aqueous inclusions with highest T_h are then interpreted to reflect most closely peak deformation/or metamorphic conditions, whereas the low-density carbonic inclusions together with pseudosecondary aqueous inclusions may represent fluids trapped during the vein formation. Finally, secondary aqueous inclusions are considered to record the conditions immediately after the veining development or the waning stage of the crack–seal process.

DISCUSSION

Development of preferred orientations of fluid inclusion trails

Many examples of the preferred orientations of fluid inclusion trails have been reported for either crystalline rocks (Pecher *et al.*, 1985; Kowallis *et al.*, 1987; Laubach, 1989; Ren *et al.*, 1989) or quartz veins and lenses (Alvarenga, 1990; Boullier *et al.*, 1991; Boiron *et al.*, 1992; Boullier and Robert, 1992; Selverstone *et al.*, 1995) or some combination of both (Cathelineau *et al.*, 1990). It is suggested that in most cases fluid inclusion trails can be regarded as excellent structural markers parallel to the average maximum principal stress direction (σ_1). This conclusion appears to be valid for trails composed of pseudosecondary fluid inclusions, as evidenced by the consistency between the orientation of set 1 trails and the established regional compression direction during orogenesis. By contrast, Cathelineau *et al.* (1990) would argue that the deviation of set 2 trails from the regional dominant shortening direction is due to reorientation of local stress fields in bulk anisotropic media, such as quartz lenses in mica schist. However, the strong preferred orientation of set 2 trails contradicts such an interpretation. Given the presence of some NE-striking D_4 folds in the regional context, set 2 trails may correspond to the compression direction of D_4 or another young deformation event.

The development of pseudosecondary fluid inclusions in fibrous quartz is not unusual in low-grade metamorphic rocks. Mullis (1987) reported an excellent example of this inclusion type for syntectonically grown Alpine quartz crystals, sometimes referred to as 'white stripes' by other workers (Roedder, 1984). Data presented in this study indicate that trails of pseudosecondary inclusions have an obvious ENE–WSW trend (set 1 in Fig. 4a). As this orientation is the bulk shortening direction interpreted for D_2, the entrapment of fluids in

this direction is implied to be a consequence of healing along tensile cracks. The trapping mechanism by which pseudosecondary inclusions formed is, in every respect, similar to that of secondary inclusions. The only difference is cracking during the growth of crystals rather than after the growth of crystals. The cause of the crystal fracturing during growth is mainly attributed to the relative instability or cycling of the effective stress levels in crack–seal deformation (Ramsay, 1980; Cox and Etheridge, 1983).

Temperature and pressure conditions during veining

In recent years fluid inclusion data obtained from syntectonic veins have been successfully used to resolve specific structural problems (Foreman and Dunne, 1991; Evans, 1995; Selverstone *et al.*, 1995). As proposed by Mullis (1987) and Nicolas (1987), fluids are systematically trapped in the growing crystal during the development of crack–seal veins and record the *P–T* evolution of the fluid from which the fibre crystallized. In many cases fluids in veins are in equilibrium with the surrounding mineral assemblages in host rocks (Crawford and Hollister, 1986; Evans, 1995). Unfortunately, the lack of fluid inclusion data in the matrix of the host rock makes it difficult to justify this assumption at Dugald River, but it is inferred that the pressure prevailing at least during early primary inclusion trapping is close to lithostatic values. Hence, detailed fluid inclusion work should provide invaluable information on deformation conditions and how they changed with time during synorogenic vein formation.

The fluid inclusions investigated in this study indicate that there is a wide variation in temperature and composition of the fluids involved during veining. The essential lack of leakage for inclusions measured precludes post-trapping modification as a reason for such a large change. At the same time, satellite inclusions or decrepitation clusters, typical of the internal overpressure re-equilibration of fluid inclusions during retrograde metamorphism (Sterner and Bodnar, 1989), have not been observed by the present author. The most likely interpretation for the wide microthermometric values is that the quartz sampled is not contemporaneous or, in other words, the inclusions investigated in this study were sequentially trapped during successive episodes of crack formation. In order to establish this history of evolution, isochores were constructed for fluid inclusions in crack–seal veins using the computer program MacFlinCor (Brown and Hagemann, 1995), together with the equation of state from Brown and Lamb (1989) for both carbonic and aqueous inclusions. Isochores for the earlier primary high-density (0.9 g cm^{-3}) $CO_2 \pm CH_4$-rich inclusions and later pseudosecondary lower-density (0.7 g cm^{-3}) CO_2-rich inclusions were constructed using peak homogenization and CO_2 melting temperatures corresponding to those in the histograms of Fig. 6. Similarly, for aqueous inclusions, isochores were generated on the basis of different peak homogenization temperatures and freezing point depressions for successive early primary, middle pseudosecondary and late secondary inclusions. The ranges of fluid densities are constrained by the isochores established using the maximum and minimum microthermometric values for each inclusion type. The isochores in Fig. 8 clearly show that *P–T* overlaps exist between different types of fluid inclusion.

The temperature and pressure conditions during veining can be estimated by means of the fluid inclusion isochores and other independently known temperature and/or pressure constraints. By comparison with data obtained from the similar mineral assemblage in the western Mount Isa Inlier (M. J. Rubenach, personal communication 1996), peak metamorphic conditions for rocks of the Lady Clayre Dolomite at Dugald River were estimated to be 450°C and 3 kbar. When plotted on the *P–T* diagram of fluid inclusions (Fig. 8), this peak temperature intersects isochore A which reflects the trapping conditions for early isolated high-density (0.9 g cm^{-3}) carbonic inclusions. In addition, the isochore for early primary aqueous inclusions (B, Fig. 8) intersects the isochore A at about 600°C. This intersec-

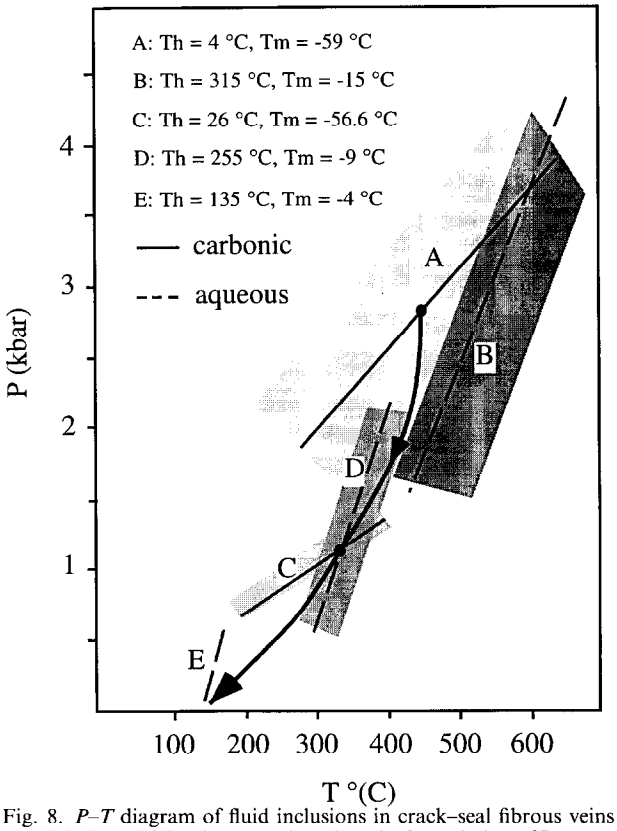

Fig. 8. *P–T* diagram of fluid inclusions in crack–seal fibrous veins at Dugald River. All isochores are based on the formulation of Brown and Lamb (1989). The shaded areas adjacent to the corresponding isochores illustrate the variations in fluid densities and *P–T* conditions. The overall *P–T* path constrained by isochores of fluid inclusions and independently known metamorphic data is convex towards the temperature axis and indicates a progressive decrease in temperature and pressure with time, implying that the formation of crack–seal veins is coeval with regional crustal uplift.

tion may be fortuitous as textural evidence indicating comtemporaneity of such early dispersed aqueous and carbonic inclusions was not found. Despite the absence of a chronological sequence between them, these early aqueous inclusions are interpreted to form somewhat later than high-density carbonic inclusions with respect to the peak metamorphism. The temperature of entrapment of such aqueous inclusions along the isochore B is unknown, but the retrograde nature of the vein suggests it was below the peak value. The mechanism by which the early primary aqueous inclusions were trapped is inferred to be syntectonic overgrowth in response to the release of elastic strain and brittle failure following accumulation of strain during crack–seal deformation (Ramsay, 1980).

In contrast, the intersection between the isochore for low-density (0.7 g cm^{-3}) CO_2-rich inclusions (C, Fig. 8) and the isochore for pseudosecondary aqueous inclusions (D, Fig. 8) can be used to define the trapping temperature and pressure under which both of these inclusions were formed as they are most likely representative of immiscible CO_2-rich and H_2O-rich fluids. Evidence used to support the presence of immiscibility is mainly derived from the observations of coexisting aqueous and CO_2-rich inclusions along the same trail (see Fig. 7). Although one might expect that trapping immiscible fluids would result in inclusions containing random mixtures of the two fluids (Craw, 1990), this is not the case at Dugald River. The immiscible fluids described in this study are most likely pure end-members of CO_2 and H_2O. Consequently, the intersection of isochores derived from two such inclusions should give both the true trapping temperature and pressure (Hagemann and Brown, 1996). Therefore, the 340°C and 1.2 kbar obtained from intersecting isochores represents the formation temperature and pressure for low-density carbonic and middle-stage aqueous inclusions. The *P–T* path must cross this point during the development of crack–seal veins. Moreover, as both of these inclusions occur along intracrystal fractures, they are considered to reflect conditions under which cracking took place during the syntectonic growth of fibres.

Finally, the isochore for secondary low-salinity aqueous inclusions (E, Fig. 8) constrains the *P–T* conditions of post-growth fluids. As most such inclusions cross-cut previous primary and pseudosecondary inclusions, they are the latest stage of fluid recorded in the veins. Compared with carbonic and moderate salinity aqueous fluids, these youngest low-salinity fluid inclusions presumably resulted from the downward percolation of meteoric water through evaporitic metasediments as crack–seal deformation accompanied uplift and the rocks approached the surface. Given that the pressure correction is not significant close to the end of regional crust uplift, the peak homogenization temperature of 130°C can be regarded as the representative temperature of the latest entrapment of fluid.

The overall *P–T* conditions during veining are characteristic of a progressive decrease in temperature and pressure with time, implying the correlation between the formation of a crack–seal vein and regional crustal uplift. This tendency is also accompanied by a density decrease for carbonic fluid ranging from early typical 0.9 g cm^{-3} to late 0.7 g cm^{-3}, and a continuous salinity decrease for aqueous fluid ranging from early typical 19 wt% NaCl, through middle 13 wt% NaCl, to late 7 wt% NaCl. It is inferred that metamorphic fluids were dominant in the early stage of veining, while meteoric water was incorporated in the late stage of the vein formation, although a precise determination of the fluid origin is beyond the scope of this study.

CONCLUSIONS

Geometrical investigation of fluid inclusion trails, combined with microthermometric data, can provide insight into the deformation conditions during orogenesis, as illustrated by fluid inclusions in syntectonic crack–seal fibrous veins in the Dugald River area. Analysis of fluid inclusion trails shows that there is strong consistency between the preferred orientations of pseudosecondary inclusion trails and the regional bulk shortening direction. However, late secondary inclusion trails generally exhibit a clockwise deviation from the inferred regional maximum principal stress and possibly correspond to a late deformation event. Moreover, the restricted distribution of secondary inclusion trails suggests that the heterogeneity resulting from crack–seal veining is not significant enough to affect the development of fluid inclusion trails as a function of the local stress reorientation at Dugald River, as demonstrated by Cathelineau *et al.* (1990) elsewhere.

Fluid inclusions within quartz fibres indicate a wide compositional variation and at least three stages of fluid entrapment during and after the development of crack–seal veins. Two general types of inclusions were distinguished: one is $CO_2 \pm CH_4$-rich and the other is H_2O-rich with low to moderate salinity (3–21 wt% NaCl). The crack–seal process was well constrained by the available microthermometric data. It initiated with the entrapment of high-density (0.9 g cm^{-3}) carbonic fluid corresponding to peak metamorphism in the host rock, followed by the formation of early aqueous inclusions during syntectonic crystallization. Afterwards, separate CO_2-rich and H_2O-rich pseudosecondary inclusions were trapped at the same time during the middle stage of the veining. The widespread presence of secondary low-salinity aqueous inclusions is regarded as the termination of the whole process.

Episodic entrapment of different fluids delicately records the nature of crack–seal deformation, that is, accumulation of elastic strain followed by brittle failure, release of strain and deposition of dissolved material. On the other hand, the wide variation in homogenization and melting temperatures for each type of inclusion, together with considerable *P–T* overlaps in isochores, suggests

changes in deformation conditions with time. A post-peak decrease in temperature, pressure, CO_2 density and salinity implies that the vein formation probably corresponds to regional crustal uplift. It is inferred that the fluids trapped in the early stages were metamorphically derived and the late-stage low-salinity aqueous fluid resulted from the downwards convection of meteoric water following regional uplift.

Finally, an important result of the present study is that trails of pseudosecondary fluid inclusions in the crack–seal fibrous veins conform to other geological settings; namely, they are reliable structural markers. Fluid inclusion data obtained from crack–seal fibrous veins can provide valuable information on the evolution of deformational/metamorphic conditions for low-grade metamorphic terrains.

Acknowledgements—Thanks go to Tim Bell for supervising this work and for criticizing earlier drafts of this paper. An acknowledgement also goes to CRA Exploration Pty Limited for providing assistance during field work and for the permission of the publication of this paper. I would like to express my gratitude to Brett Davis and Aaron Stallard for their valuable comments on an earlier version of the manuscript. Thorough and constructive reviews by two Journal reviewers assisted greatly in removing discrepancies and suggesting alternatives. Also, editorial comments made by Associate Editor Richard Norris are greatly appreciated. The author was the recipient of a James Cook University Ph.D Scholarship for the duration of this research.

REFERENCES

de Alvarenga, C. J. S. (1990) Chronology and orientations of N_2–CH_4, CO_2–H_2O-rich fluid inclusion trails in intrametamorphic quartz veins from the Cuiaba gold district, Brazil. *Mineralogical Magazine* **54**, 245–255.

Beardsmore, T. J., Newbery, S. P. and Laing, W. P. (1988) The Maronan Supergroup—an early volcanosedimentary rift sequence in the Mount Isa Inlier, and its implications for ensialic rift in the middle Proterozoic of northwestern Queensland. *Precambrian Research* **40**, 487–507.

Blake, D. H. (1982) A review of the Corella Formation, Mount Isa Inlier, Queensland. *Journal of Australian Geology and Geophysics* **7**, 113–118.

Bodnar, R. J. (1993) Revised equation and table for determining the freezing point depression of H_2O–NaCl salinity. *Geochimica et Cosmochimica Acta* **57**, 683–684.

Boiron, M. C., Essarraj, S., Sellier, E., Cathelineau, M., Lespinasse, M. and Poty, B. (1992) Identification of fluid inclusions in relation to their host microstructural domains in quartz by cathodoluminescence. *Geochimica et Cosmochimica Acta* **56**, 175–185.

Boullier, A. M., Lanord, C. F., Dubessy, J., Adamy, J. and Champenois, M. (1991) Linked fluid and tectonic evolution in the High Himalaya mountains (Nepal). *Contributions to Mineralogy and Petrology* **107**, 358–372.

Boullier, A. M. and Robert, F. (1992) Palaeoseismic events recorded in Archaean gold–quartz networks, Val d'Or Abitibi, Quebec, Canada. *Journal of Structural Geology* **14**, 161–179.

Brown, P. E. and Hagemann, S. G. (1995) MacFlinCor and its application to fluids in Archaean lode-gold deposits. *Geochimica et Cosmochimica Acta* **59**, 3943–3952.

Brown, P. E. and Lamb, W. M. (1989) P–V–T properties of fluids in the system H_2O–CO_2–NaCl: new graphical presentations and implications for fluid inclusion studies. *Geochimica et Cosmochimica Acta* **45**, 1209–1221.

Cathelineau, M., Lespinasse, M., Bastoul, A. M., Bernard, L. and Leroy, J. (1990) Fluid migration during contact metamorphism: the use of oriented fluid inclusion trails for a time/space reconstruction. *Mineralogical Magazine* **54**, 169–182.

Cox, S. F. and Etheridge, M. A. (1983) Crack–seal fibre growth mechanisms and their significance in the development of oriented layer silicate microstructures. *Tectonophysics* **92**, 147–170.

Craw, D. (1990) Fluid evolution during uplift of the Annapurna Himal, central Nepal. *Lithos* **24**, 137–150.

Crawford, M. L. and Hollister, L. S. (1986) Metamorphic fluids: the evidence from fluid inclusions. In *Fluid–Rock Interactions During Metamorphism*, ed. J. V. Walther and B. J. Wood, pp. 1–35. Springer, New York.

Derrick, G. M., Wilson, I. H. and Hill, R. M. (1977) Revision of the stratigraphic nomenclature in the Precambrian of northwestern Queensland, VII: Mount Albert Group. *Queensland Government Mining Journal* **78**, 113–116.

Evans, M. A. (1995) Fluid inclusions in veins from the Middle Devonian shales: a record of deformation condition and fluid evolution in the Appalachian Plateau. *Bulletin of the Geological Society of America* **107**, 327–339.

Foreman, J. L. and Dunne, W. M. (1991) Conditions of vein formation in the southern Appalachian foreland: constraints from vein geometries and fluid inclusions. *Journal of Structural Geology* **13**, 1173–1183.

Hagemann, S. G. and Brown, P. E. (1996) Geobarometry in Archaean lode-gold deposits. *European Journal of Mineralogy* **8**, 937–960.

Holcombe, R. J., Pearson, P. J. and Oliver, N. H. S. (1991) Geometry of a middle Proterozoic extensional detachment surface. *Tectonophysics* **191**, 255–274.

Holcombe, R. J., Pearson, P. J. and Oliver, N. H. S. (1992) Structure of the Mary Kathleen Fold Belt. In *Detailed Studies of the Mount Isa Inlier*, ed. A. J. Stewart and D. H. Blake, pp. 257-287. Australian Geological Survey Organization Bulletin **243**.

Kowallis, B. J., Wang, H. F. and Jang, B. A. (1987) Healed microcrack orientations in granite from Illinois borehole UPH-3 and their relationship to the rock's stress history. *Tectonophysics* **135**, 297–306.

Laubach, S. E. (1989) Palaeostress directions from the preferred orientation of closed microfractures (fluid-inclusion planes) in sandstone, Eastern Texas basin, U.S.A. *Journal of Structural Geology* **11**, 603–611.

Lespinasse, M. and Pecher, A. (1986) Microfracturing and regional stress field: a study of the preferred orientations of fluid inclusion planes in a granite from the Massif Central France. *Journal of Structural Geology* **8**, 169–180.

Mullis, J. (1987) Fluid inclusion studies during very low-grade metamorphism. In *Low Temperature Metamorphism*, ed. M. Frey, pp. 162–199. Blackie, London.

Newbery, S. P., Carswell, J. T., Allutt, S. L. and Mutton, A. J. (1993) The Dugald River zinc–lead–silver deposit: an example of a tectonised Proterozoic stratabound sulphide deposit. *Australasian Institute of Mining and Metallurgy Publication Series* n.7/93. 7–21.

Nicolas, A. (1987) *Principles of Rock Deformation*. Reidel, Dordrecht.

Oliver, N. H. S., Holcombe, R. J., Hill, E. J. and Pearson, P. J. (1991) Tectono-metamorphic evolution of the Mary Kathleen Fold Belt, northwest Queensland: a reflection of mantle plume processes? *Australian Journal of Earth Sciences* **38**, 425–456.

Pecher, A., Lespinasse, M. and Leroy, J. (1985) Relations between fluid inclusion trails and regional stress field: a tool for fluid chronology—An example of an intragranitic uranium ore deposit (northwest Massif Central France). *Lithos* **18**, 229–237.

Ramsay, J. G. (1980) The crack–seal mechanism of rock deformation. *Nature* **284**, 135–139.

Ramsay, J. G. and Huber, M. I. (1983) *The Techniques of Modern Structural Geology, Volume 1: Strain Analysis*. Academic Press, London.

Reinhardt, J. (1992) The Corella Formation of the Rosebud Syncline (central Mount Isa Inlier): deposition and metamorphism. In *Detailed Studies of the Mount Isa Inlier*, ed. A. J. Stewart and D. H. Blake, pp. 229-256. Australian Geological Survey Organization Bulletin **243**.

Ren, X., Kowallis, B. J. and Best, M. G. (1989) Palaeostress history of the Basin and Range province in the western Utah and eastern Nevada from healed microfracture orientations in granites. *Geology* **17**, 487–490.

Roedder, E. (1984) Fluid inclusions. In *Reviews in Mineralogy*, Vol. 12. ed. P. H. Ribbe. Mineralogical Society of America.

Selverstone, J., Axen, G. J. and Bartley, J. M. (1995) Fluid inclusion constraints on the kinematics of footwall uplift beneath the Brenner Line normal fault, Eastern Alps. *Tectonics* **14**, 264–278.

Shepherd, T. J., Rankin, A. H. and Acdenton, D. H. M. (1985) *A Practical Guide to Fluid Inclusion Studies*. Blackie, London.

Sterner, S. M. and Bodnar, R. J. (1989) Synthetic fluid inclusions—VII. Re-equilibration of fluid inclusions in quartz during laboratory-simulated metamorphic burial and uplift. *Journal of Metamorphic Geology* **7**, 243–260.

Valenta, R. K. (1989) Vein geometry in the Hilton area, Mount Isa, Queensland: implications for fluid behaviour during deformation. *Tectonophysics* **158**, 191–207.

Valenta, R. K., Cartwright, I. and Oliver, N. H. S. (1994) Structurally-controlled fluid flow associated with breccia vein formation. *Journal of Metamorphic Geology* **12**, 197–206.

Winsor, C. N. (1983) Syntectonic vein and fibre growth associated with multiple slaty cleavage development in the Lake Moondara area, Mount Isa, Australia. *Tectonophysics* **92**, 195–210.

Xu, G. (1996) Structural geology of the Dugald River Zn–Pb–Ag deposit, Mount Isa Inlier, Australia. *Ore Geology Reviews* **11**, 339–361.